Solar-minimum quiet-time ion energization and outflow in dynamic boundary related coordinates

W.K. Peterson[1], L. Andersson[1], B.C. Callahan[1], H.L. Collin[2], J.D. Scudder[3], and A.W. Yau[4]

[1]Laboratory for Space and Atmospheric Science, University of Colorado, Boulder
[2]Lockheed Martin ATC, B/255, ADCS, 3251 Hanover St., Palo Alto, California 94304
[3]Department of Physics and Astronomy, University of Iowa, Iowa City
[4]Department of Physics and Astronomy, University of Calgary, Alberta, Canada

Abstract

We report hemispheric average fluxes and energies of outflowing energetic ($0.015 < E/q < 33$ keV) H^+, O^+, and He^+ ions in dynamic boundary-related coordinates, from observations obtained by the Polar/TIMAS instrument near 6,000 km altitude in the southern hemisphere during quiet geomagnetic intervals at solar minimum.

We discuss our observations in terms of known energization and transport processes. We find that only a small fraction of energetic ions escape from the ionosphere directly into the polar cap and at quiet times the characteristic energies of escaping H^+ are between 30 and 300 eV in the cusp region and between 30 eV and 1.2 keV in the midnight sector. For O^+ we conclude the characteristic energy in the cusp is ~100 eV and between 150 and 600 eV in the midnight sector. Our data suggest that the relative energization and acceleration of O^+ is significantly different in the noon quadrant. The observations and analysis presented here also suggest that O^+ has activity dependent transport paths from the ionosphere to the ring current that have not previously been identified.

Introduction

The ionosphere is mass coupled to the magnetosphere by the fluxes of escaping light and heavy ions and less intense but more energetic fluxes of precipitating ions of both solar wind and ionospheric origins. Heavy ions such as O^+ have transit times from the ionosphere through the plasma sheet to the ring current that are long compared to substorm time scales. The energization and transport of ionospheric O^+ is of interest because O^+ ions are believed to reduce reconnection rates [e.g. Shay and Swisdak, 2004, Hesse and Birn, 2004] and modify the pressure distribution in the ring current, thus modifying the evolution of large geomagnetic storms [e.g. Brandt et al. 2002, and Delcourt et al. 2002].

Understanding where and how energy is transferred to thermal heavy ions is central to understanding magnetosphere-ionosphere interactions. Comprehensive summaries of *in-situ* observations of the ionospheric sources of magnetospheric plasma are available; see

Hultqvist et al., [1999], Cully et al., [2003], Lennartsson et al., [2004], Andersson et al., [2004, 2005], Nilsson et al., [2006], Ebihara et al., [2006], Peterson et al., [2006] and Lotko, [2007] for recent reports. These observations however do not have adequate coverage (temporal, or spatial) to resolve details of the energization and transport of O^+ from the ionosphere to the plasma sheet, magnetopause, or ring current.

Observational information about the O^+ ring current plasma is similarly limited. Almost all of the ring current plasma comes from the plasma sheet, which in turn comes from the ionosphere and solar wind. (See, for example, Hultqvist et al., 1999). During geomagnetic storms, the ring current contains a significant population of energetic O^+ that modifies the pressure balance in the region as well as the dynamics and evolution of the ring current. (See, for example, Fok et al., 2001, or Khazanov et al., 2007.) The best empirical model of ring current O^+ [Roeder et al., 2005] does not include ring current dynamics. Recent global images from space have shown that O^+ injection into the ring current is episodic and related to sub-storms [e.g. Mitchell et al., 2003]. However, it is difficult to derive detailed O^+ ring current distributions from global images, because the derivation relies heavily on assumptions that are derived from global magnetospheric models. Indeed, the models used to interpret energetic neutral atom (ENA) images have to make assumptions about the ring current O^+ source population in the plasma sheet, or equivalently the physics associated with the energization and transport of O^+ to the plasma sheet. (See for example, Perez et al., 2004.)

Because direct observations on the time scales of interest are not available to resolve questions about the temporal evolution of O^+ energies and densities in relevant regions of the magnetosphere, investigators must rely on large-scale models to infer ion transport paths, energization regions, and pressure distributions from sparse data.

One way to improve the usefulness of the limited observations of the energy and fluxes of ions leaving the ionosphere is to report the fluxes and energies in dynamic, boundary-related coordinates. See, for example Andersson et al., [2004, 2005]. Casting outflow in boundary-related coordinates removes some of the "smearing" of average outflow data thus making them more realistic as model inputs and/or model validation data.

Here we recast in dynamic boundary related coordinates the observations of ion outflow fluxes and energies obtained on the Polar spacecraft by the Toroidal Imaging Mass Angle Spectrograph (TIMAS) [Shelley et al., 1995] reported by Peterson et al. [2001, 2006] and Lennartsson et al. [2004]. Our observations are restricted to geomagnetically quiet intervals characterized by D_{ST} values above -50 nT. The analysis reported below suggests the existence of different O^+ transport paths from the ionosphere to the ring current during geomagnetic active and quiet times.

Data

The data in this report were acquired near Polar perigee between 5,000 and 7,000 km altitude from March 1996 until December 8, 1998. Because six months are required to obtain data from all local times, and geomagnetic storms are not uniformly distributed in time, we have excluded intervals of intense geomagnetic activity (i.e. Dst < -50 nT) from the average data reported below. Data after December 8, 1998 were not included because

of a high voltage breakdown event in the TIMAS instrument that resulted in reduced sensitivity and energy range.

We used electron and ion observations with 15 s temporal resolution from the Polar/Hydra instrument [Scudder et al., 1995] to identify the equatorward and poleward boundaries of the auroral oval, following the procedure pioneered for low orbiting satellites by Sotirelis and Newell [2000] and adapted to high altitude satellites by Andersson et al. [2004]. The times of poleward boundary crossings of the auroral oval are derived from the energy and angular distributions of ~100 eV electrons. The times of equatorward boundary crossings of the auroral oval are identified from observations of the loss cones in the energetic (>1 keV) ion distributions.

We then used these times to reorganize the TIMAS data reported by Peterson et al. [2001, 2006] and Lennartsson et al. [2004], as follows. The TIMAS instrument is sensitive to ions in the energy range from 15 eV/e to 33 keV/e [Shelley et al., 1995]. Parameters, including net upflowing ion flux derived from TIMAS measurement data, were organized in fixed invariant latitude (INVL) and MLT coordinates, as was done previously, and in dynamic boundary-related latitude (DBRL) and MLT coordinates, as described by Andersson et al. [2004]. Specifically the observations made in each auroral zone crossing between the times of equatorward and poleward auroral zone boundary crossings were assigned to ten DBRL bins based on the times of the observations relative to the times of boundary crossings. Likewise, for each polar cap crossing, observations are distributed into ten DBRL latitude bins based on the times of the poleward auroral crossing and the time and magnitude of the maximum invariant latitude reached by Polar. If the maximum invariant latitude reached was less than 90°, data were distributed into fewer bins closer to the polar cap boundary. The number of DBRL latitude bins filled was determined using an algorithm based on the maximum invariant latitude and the invariant latitude of the polar cap crossing. Magnetic local time for each interval was obtained from Polar ephemeris data. TIMAS data were acquired with 12-s temporal resolution, during which the Polar satellite traverses slightly less than one degree in invariant latitude at perigee.

Data from quiet geomagnetic intervals (Dst > -50) were binned both in INVL versus MLT and in DBRL versus MLT. In the fixed coordinated system, the bin size is 2° by 2 hours. In the dynamic boundary-related coordinate system, as noted above, we use 10 boundary-related latitude (BL) bins and two-hour magnetic local time (MLT) bins in both the auroral zone and polar cap, respectively. The bin sizes were selected to minimize artifacts introduced by the interpolations involved in binning.

Figure 1 shows the number of samples in both coordinate systems. Figure 1 shows that we have over 100 samples in all but the poleward-most polar cap sampling bin. The relative minimum between 60° and 65° invariant latitude in the static coordinate system is the result of two factors. First, the Polar perigee was near the pole and so there are more samples per bin as the satellite slows down as it goes away from the pole (perigee). Second, intervals excluded from analysis because of high background count rate due to radiation belt particles are typically found near 60° INVL. The data in boundary-related latitude coordinates reported here are a subset of the data reported in fixed invariant latitude coordinates. There are fewer samples per bin in boundary coordinates because it was not possible to identify both poleward and equatorward boundaries on every auroral

zone crossing. In addition, the range of invariant latitude within the auroral zone and polar cap typically does not extend below 65° or above 80° INVL.

Figure 2 shows the hemispheric net outward flux of H$^+$, O$^+$ and He$^+$ observed during quiet conditions for the interval of interest. The method used to calculate the net upward fluxes reported here is the same as described in Peterson et al. [2001, 2006]. Explicitly, the number flux is the integral of the measured differential number flux over energy and solid angle, normalized to the 300 km reference altitude. A correction has been made for energetic ions precipitating into the ionosphere (i.e. absorbed and not reflected). This component has a net downflow, which causes the outflow to be underestimated. The correction was made by calculating the net outflow rate that would have corresponded to a nominal loss cone filled with the observed downward field aligned ion flux. Correcting for the precipitation downflow resulted in a significant but not overwhelming increase in the total net outflow rate in the H$^+$ but little change in the other species. The correction is largest equatorward of the auroral zone.

The top panels in Figure 2 show the flux in the static coordinate system, as a function of MLT and fixed invariant latitude, and reproduce the data reported in the top row of Figure 1 of Peterson et al. [2006]. However here the MLT bins are 2 hours wide and the INVL bins are 2° wide and extend to 54°. The large black areas equatorward of about 70° correspond to regions where the net fluxes are downward. In contrast, the bottom panels show the flux in the dynamic boundary-related coordinate system, as a function of MLT and boundary-related latitude.

It is important to note that the average shape of the auroral oval is not circular as depicted in the bottom panels of Figure 2 and other figures presented in this paper. The auroral oval is narrowest near noon and widest near midnight. The width of the auroral oval varies at all times and increases with increasing geomagnetic activity. See, for example, Feldstein [1963], Holzworth and Meng [1975], and Andersson et al., [2004]. The Holzworth and Meng representation of the auroral oval for the third of seven activity levels shows that ~9% of the auroral zone area is in the noon sector, ~47% in the midnight sector, and the remaining area in the dawn and dusk sectors.

Understanding where and how escape energy is transferred to thermal heavy ions is central to understanding magnetospheric-ionospheric interactions. Heavy ions such as He$^+$ and O$^+$ have thermal energies much less than 1 eV in the ionosphere. They must acquire additional energy to escape the ionosphere and enter the magnetosphere. Escape velocity from the Earth's topside ionosphere is 11 km/s or 10 eV for O$^+$ and 2.5 eV for He$^+$. To overcome gravity and reach the altitude where the data reported here were acquired He$^+$ and O$^+$ ions must acquire at least half of their escape energy.

A large fraction of the energy necessary for heavy ion escape is believed to be provided by plasma processes that directly heat or accelerate ions. Above the dense, neutral particle-dominated ionosphere, these processes leave the locally accelerated or heated ions with characteristic energy and angular distributions. Ions accelerated upward parallel to the magnetic field have distributions in a restricted energy range that are peaked around the magnetic field direction. These are the so-called ion beam distributions. Ions that are heated or energized by plasma waves are in general not restricted in energy and have angular distributions that are peaked at angles away from the magnetic field

direction. These are the so-called ion conic distributions. Because the magnetic field intensity decreases with altitude, conservation of the first adiabatic invariant leads to ion conic distributions converting into ion beam like distributions at higher altitudes. Because of the "folding" of ion conic distributions with altitude and the finite angular response of ion detectors, it is generally not possible to separate ion beam and conic distributions. In any case, the existence of ion distributions peaked in angle is a clear signature that ions have been accelerated and/or heated above the ionosphere and below the point of observation. Here we call these distributions upflowing ion (UFI) distributions.

Figure 3 presents the net upflowing flux from UFI distributions, i.e. the subset of intervals shown in Figure 2 that have well-defined peaks in their angular distributions. As discussed in Peterson et al. [2006] and Collin et al. [1998] data have been separated into three broad energy bands: 0.015-0.3, 0.3-4, and 4-33 keV, respectively. We then examined the ion pitch-angle distribution in each energy band in each 12-s measurement interval, to determine the presence of a peak in the distribution in which (1) the full angular width at half maximum is less than 45°, (2) the peak flux is greater than 10^{10} ions/m^2-s-sr, and (3) the peak flux is above the energy-dependent noise threshold. For the southern hemisphere data considered here, UFI distributions are defined as having pitch angle peaks in the range of 0° to 75°. Figure 3 displays the net upward flux from all 12-s accumulation intervals with a peak in the angular distribution in one of these energy bands. Visual comparison of the data in Figures 2 and 3 shows that a relatively large fraction of the net upflowing O^+ fluxes seen in Figure 2 is from UFI events, i.e. intervals where there was significant ion energization or acceleration above altitudes of ~1000 km.

Table 1 shows the net upflowing hemispheric fluxes for different MLT and invariant latitude regions shown in Figures 2 and 3 in units of 10^{24} ions s^{-1}. For each mass species, it shows the flux of all ions (columns 4-8) and only UFI (columns 9-13), respectively, as well as the latter as a percentage of the former (columns 14-18). In each case, it shows the integrated flux at all latitudes in the static (fixed invariant latitude) coordinate system (first row in each species), and the flux at all latitudes, in the polar cap, and in the auroral zone, respectively, in the dynamic (boundary-related) coordinate system (second to fourth row), as well as the polar cap flux as a percentage of the flux at all latitudes (last row).

For data in the dynamic boundary-related coordinates, the area over which net outflowing flux was distributed was obtained using the Holzworth and Meng [1975] algorithm for auroral boundaries for the third of seven activity levels. The relative percentage of He^+ UFI fluxes shown is lower than that reported for H^+ and O^+. This is attributed to the fact that He^+ data were usually collected on the spacecraft with lower energy resolution.

Table 1 shows anomalously high percentages of UFI for H^+ and O^+ in static coordinates for some MLT quadrants. This is because all of the UFI fluxes are upflowing by selection, whereas the net fluxes include mirroring energetic ions. The smaller net fluxes are the result of an imperfect correction for the net flux associated with precipitating energetic ions that are not mirrored but rather absorbed in the ionosphere. This point is addressed further in the discussion section below.

Table 1 also shows that only a negligible fraction (~2-3%) of the outflowing energetic ions observed by TIMAS is in the polar cap.

Because the relative percentage of the flux associated with upflowing ion (UFI) events in all regions is large, we conclude that the majority of upflowing ions observed by TIMAS have received significant energy above the ionosphere.

The data in Table 1 do not include ion fluxes with energies less than 15 eV. Table 2 compares the net outflowing fluxes of energetic ions in boundary-related coordinates reported in Table 1 with previous observations of fluxes of upflowing energetic and thermal ions, including the polar wind. The total net outflowing rate shown in the fourth, seventh and tenth column, respectively, is from the source noted in the first column, and was obtained at the altitude given in the second column over the energy range indicated in the third column. The total outflowing rates reported from Akebono, DE, and Polar/TIMAS were derived from long term averages of outflowing fluxes in fixed INVL/ MLT coordinates. The outflow rates reported from FAST were obtained in DBRL / MLT coordinates. The total outflowing fluxes from the Polar/TIDE instrument were obtained from the flux values given in the review by Yau et al., [2007, Table 3] using areas derived from the Holzworth and Meng [1975] for the third of seven activity levels. These are likely overestimates because we have assumed that the entire polar cap and auroral zone are uniformly filled with the constant flux of thermal ions indicated. The overestimate is nevertheless useful because it allows us to estimate the relative magnitudes of the thermal and energetic ion fluxes.

Yau et al., [2007] reviewed polar wind observations and noted the considerable uncertainty in the magnitude of the polar wind densities and velocities arising both from observational constraints and real variability. We view the factor of ~6 difference in the total upwards fluxes obtained at 5,000 and 50,000 km reported in Table 2 as consistent with the variability of the polar wind, episodic sampling particularly at 50,000 km, and transport of O^+ from lower latitudes.

Table 2 estimates the fractions of outflowing ions below 15 eV under the assumptions noted. These fractions were determined from the ratio of the quoted thermal outflow rates from Polar/TIDE to the sum of thermal and energetic fluxes. The estimates based on the observations of Su et al. [1998] at Polar perigee (5,000 km) and apogee (50,000 km), respectively, are reported separately. The fluxes derived from Akebono ion mass spectrometer data [Whalen et al., 1990, Cully et al., 2003] cover the energy range from 0 to 70 eV. It is extremely difficult to estimate the flux of upflowing ions with energies between 15 and 70 eV, so Table 2 does not include an estimate of the fraction below 15 eV in the Akebono data.

Estimates of the characteristic energies of escaping ions provide information on the processes responsible for energizing and transporting them. Lennartsson et al. [2004] and Peterson et al. [2006] estimated characteristic energies of escaping ions from the ratio of the observed energy flux to the observed number flux in the TIMAS energy range. Figure 4 presents the distribution of characteristic energy derived from the ratio of energy flux to number flux in dynamic boundary-related coordinates for the total fluxes shown in Figure 2 and the UFI fluxes shown in Figure 3. The derived characteristic energy is encoded in the color bar on the right. Black pixels indicate latitude - MLT bins where the uncertainty in the characteristic energy is outside of the 95% confidence interval based on observed counting rates.

The energies shown in Figure 4 are upper limits because the TIMAS data used to calculate the energies does not include the significant flux of ions below 15 eV. Table 3 reports the characteristic energies for H^+, O^+ and He^+ in the polar cap (PC) and auroral zone (AZ), estimated with and without including thermal ion fluxes reported in Table 2, respectively. The third column in Table 3 shows the average ratio of energy flux to number flux within the TIMAS energy range taken over all MLT. The fourth column reports the same ratio for the UFI for comparison. Assuming the characteristic energy of the upflowing thermal flux in the fifth column to be 1 eV, the characteristic energy of the combined thermal and energetic fluxes is estimated in the sixth column. The resulting energies are lower than the TIMAS threshold (15 eV) in the polar cap, indicating that thermal outflow, i.e. the polar wind, dominates in the polar cap region.

Table 4 reports the characteristic energy for H^+, O^+ and He^+ shown in Table 3 in the different MLT quadrants of the auroral zone. We discuss the importance of the anomalously high O^+ UFI percentage in the noon quadrant below.

Discussion

We have presented quantitative measures of outflowing fluxes and characteristic energies of H^+, O^+, and He^+ during geomagnetically quiet intervals (Dst > -50) in dynamically determined auroral zone and polar cap. We used data from the Polar/Hydra instrument [Scudder et al. 1995] and procedures developed for FAST by Andersson et al. [2004] to identify the times that the Polar satellite crossed auroral boundaries. The polar cap boundary crossing times were derived from electron measurements and the equatorward boundary crossing times were derived from ion data. These times were then used to cast previously reported data from the Polar/TIMAS instrument into the dynamic boundary-related latitude versus MLT coordinate system described above. Figure 2 shows that, during the geomagnetically quiet intervals considered here, the midnight auroral oval extends to ~65° INVL and the dayside to ~70° as expected.

Escaping ionospheric ions.

The net hemispheric escaping fluxes of H^+, O^+, and He^+ reported in fixed INVL/MLT coordinates in Table 1 are slightly less than those reported by Peterson et al. [2006] and Lennartsson et al. [2004] from the same data set. In addition, the percentage of O^+ and H^+ ions accelerated above the ionosphere (i.e. the UFI events presented in Figure 3 and Table) in the dusk quadrant is anomalously high in fixed INV/MLT coordinates but not in dynamic coordinates. These differences arise because of the imperfect correction for the net flux associated with precipitating energetic ions that are not mirrored but rather absorbed in the ionosphere, and the lower latitude limit (54º) of invariant latitude used here. Lennartsson et al. [2004] showed that corrections for energetic ions missing in the upflowing loss cone population are largest below ~65° INVL. Figure 2 shows that almost all of the data reported in the dynamic boundary-related coordinates are acquired above 65° INVL.

Table 1 shows some differences in the local time distributions between the fixed invariant latitude and the dynamic boundary-related coordinates. For example the dawnward quadrant of H^+ outflow in boundary-related coordinates is about half that in the fixed coordinates and there are slightly smaller differences in all but the dusk quadrant of O^+ outflow. We attribute these differences to the relatively small areas and modest fluxes in the dawn and dusk sectors of the auroral zone in dynamic coordinates.

In boundary coordinates, Table 1 shows that 32, 40, and 20 percent respectively of the auroral flux of escaping H^+, O^+, and He^+ energetic ions comes from the noon quadrant at quiet times. These ratios are similar to those reported in fixed coordinates by Peterson et al. [2006]. Other investigators (e.g. Strangeway et al., [2005], and Zheng et al., [2005]) have shown that most of the escaping ions in the noon quadrant are on cusp field lines and that significantly more ions escape during geomagnetically active times.

Figure 2 and Table 1 show that a small (~2-3%) fraction of energetic ions escaping the ionosphere are in the polar cap at the 1 R_E altitude sampled by Polar. A fraction of these ions originated in the auroral zone and were driven into the mid altitude polar cap by convection electric fields. Table 1 reports a similar percentage of fluxes associated with UFI events in the polar cap. As noted above, UFI distributions indicate that significant energy has been acquired above the ionosphere. Because the relative percentage of the flux associated with upflowing ion (UFI) events shown in Table 1 is large, we conclude that the majority of upflowing ions observed by TIMAS have acquired significant energy above the ionosphere. Table 1 shows that the MLT average percentage of UFI events in the polar cap is comparable to that in the aurora. Table 1 also shows that UFI events are found in the central polar cap. We therefore conclude that some of the energetic ions seen in the polar cap by TIMAS are associated with acceleration and/or heating events and not with the polar wind. This confirms earlier reports [e.g. Shelley et al., 1982] that energetic ions observed in the polar cap are not only transported there by prevailing convection electric fields, but are also produced by ion acceleration events occurring in the polar cap ionosphere.

Cully et al. [2003] and Peterson et al. [2006] noted that variations in estimates of escaping ionospheric ions were consistent with significant fluxes outside of the energy ranges of the instruments. In the case of Akebono, the missing fluxes were above the 70 eV upper energy limit of the instrument. In the other cases, the missing fluxes were below instrumental low energy thresholds. Table 2 shows that after consideration of the TIMAS energy range, the results presented here in boundary-related coordinates are consistent with previous reports of net outflowing ionospheric ions obtained from Dynamics Explorer -1, FAST, Akebono, and Polar.

We report in Table 2 estimates of the relative fraction of thermal ions with energies below the 15 eV TIMAS threshold but still energetic enough to reach the plasma sheet. Two estimates of hemispheric thermal ion outflow including both the auroral zone and the polar cap are given. These estimates are based on observations made from the TIDE instrument on the Polar satellite reported by Su et al., [2001]. The estimates assume that the reported ion fluxes at both 5,000 and 50,000 km are constant and uniform over the auroral oval and the polar cap. The thermal ion outflow estimates in Table 3 are systematically high because of the known dependence of polar wind fluxes on solar illumination (See, for example Su et al., 2002 and Yau et al., 2007), energization of an

unknown fraction of thermal ions in the auroral zone, and convection of thermal ions into the auroral zone from the plasmasphere. The relative magnitudes of these effects are expected to be different at different altitudes, which can explain some, if not all, of the differences in the estimates of hemispheric thermal ion outflow based on TIDE observations at 5,000 and 50,000 km shown in Table 2.

In spite of the limitations introduced by imprecise estimates of the flux of thermal ions with sufficient energy to reach the plasma sheet, the data presented in Table 2 allow us to conclude that a larger fraction of O^+ is energized above 15 eV at altitudes near Polar perigee (~6,000 km), compared with H^+. This is consistent with the result reported by Peterson et al. [2006] and suggests that auroral and cusp energization processes acting between the ionosphere and Polar perigee at ~6,000 km have significant mass dependencies.

Characteristic energies of escaping ionospheric ions

We know surprisingly little about the average energy of ionospheric ions escaping the ionosphere even during geomagnetically quiet intervals. This information is needed to improve models that can be used to systematically explore feedback paths that relate ionospheric outflows and long time-scale magnetospheric processes such as storms and substorms. These models are needed to unravel the complex dynamics during the transition from geomagnetically quiet intervals to geomagnetically active intervals, where slow heavy ions in transit between the ionosphere, plasma sheet, and ring current can have large effects. The reason it is difficult to determine characteristic energies of escaping ions is that they co-exist on auroral field lines with trapped ions. The relatively few papers reporting characteristic energies of escaping ionospheric ions (e.g. Collin et al., [1981], Peterson et al., [1992], Miyake et al., [1993], Lennartsson et al., [2004], Andersson et al., [2005], Nillson et al., [2006], and Peterson et al., [2006]) have used several different approaches to estimate characteristic energy.

Most estimates of escaping energy have been made on the basis of events selected by virtue of their ion angular distributions being peaked in the upward direction, and events selected primarily from intervals of moderate to intense geomagnetic activity. The early reports [Collin et al., 1981 and Miyake et al., 1993] were limited by the number of events the investigators could visually identify in the data. Later reports used automated detection of events (e.g. Peterson et al., [1992] and Andersson et al., [2005]) but did not include H^+ because of the intense trapped H^+ population. Lennartsson et al., [2004], Peterson et al., [2006] and we obtain estimates of characteristic energies of escaping ions from ratios of energy flux to number flux. As noted in these papers complications arising from corrections for the trapped ion component, large regions of net downward flux below 65° invariant latitude, and significant fluxes below the 15 eV TIMAS threshold complicate the direct interpretation of the ratios as a characteristic energy.

Tables 3 and 4 summarize the characteristic energies derived using three methods: (1) ratios of TIMAS observed energy flux to number flux, (2) ratios of TIMAS data restricted to UFI events, and (3) ratios including estimates of the thermal energy and number flux below 15 eV not detected by the TIMAS instrument. The first two methods

overestimate the characteristic energy, because thermal fluxes below 15 eV are not included. The third method underestimates the characteristic energy in the auroral zone because we overestimate the thermal flux in the auroral zone.

Because only a small fraction of escaping ionospheric ions detected by the TIMAS instrument is found in the polar cap, and because the outflowing fluxes in the polar cap are dominated by thermal plasma, it is not possible to obtain reliable estimates of the characteristic energy of escaping ions in the polar cap from the TIMAS data presented here. This is confirmed in Table 3, which shows that characteristic energies in the polar cap vary widely depending on the method used to estimate them.

Table 4 shows characteristic energies in the dynamically determined auroral zone for four MLT quadrants. The characteristic energy of H^+ UFI events in the dawn and dusk sectors is significantly lower than that of all H^+ ions; likewise, the energy of UFI events in the noon and midnight sectors is also somewhat lower. No such pattern is seen in the O^+ and He^+ energies. This systematic difference between relative energies could be real, or could be the result of errors in the correction for the precipitating fraction of the trapped ion distributions. (See the description of Figure 2 above). In any case, the ratios from both the full data set and the UFI-restricted subset are upper limits on the characteristic energy. We conclude that at quiet times near the Polar perigee altitude of ~6,000 km, the characteristic energies of escaping H^+ are between 30 and 300 eV in the cusp region and between 30 eV and 1.2 keV in the midnight sector. For O^+ we conclude that the characteristic energy is ~100 eV in the cusp and between 150 and 600 eV in the midnight sector. These are the first estimates for the energy of escaping ions that include both the thermal and energetic components of the distributions.

Table 1 shows that compared to H^+ and He^+ an anomalously high (76%) percentage of the O^+ fluxes observed in the noon auroral zone quadrant are associated with ion acceleration (UFI) events. There are smaller differences in other MLT quadrants, but they are not quite as large. This difference suggests that the relative energization and acceleration of O^+ in the noon quadrant is significantly different from those in the MLT quadrants. It follows that, in large scale multi-fluid codes, care must be taken in parameterizing O^+ energization as a function of MLT.

Implications of the results reported here

Because of limitations of the data set and the D_{ST} index, we have not extended our analysis to higher levels of D_{ST} or subdivided the data presented here into smaller D_{ST} bins. Nevertheless, observations reported here supplemented by those from other instruments on the Polar, FAST, and International Sun-Earth Explorer (ISEE) -1satellites suggest that energization and transport of O^+ from the ionosphere to the plasma sheet is activity dependent. As reported in Figure 2, O^+ fluxes during geomagnetically quiet (D_{ST} > -50) intervals originate on auroral field lines at all magnetic local times. Most of the O^+ ions flowing up auroral field lines are transported to the plasma sheet. Magnetic field lines very close to noon and near midnight are connected to the mid-plane ($GSM_Y \cong 0$) of the plasma sheet. O^+ ions leaving the ionosphere on field lines away from noon or midnight are transported to the flanks of the plasma sheet. During active times, the O^+ flux intensity near noon and midnight significantly increases; see, for example, Tung et

al., [2001], Strangeway et al., [2005], or Zheng et al., [2005]. This increase in outflow near noon and midnight is consistent with a relative increase in the O^+ plasma sheet energy and density near $GSM_Y \cong 0$ reported by Lennartsson and Shelley [1986] during geomagnetically active times.

Our current understanding of ring current region dynamics is based primarily on large-scale models that have been validated by sparse in-situ observations and global ENA images, the interpretations of which are model dependent. All models have to make assumptions about the ring current O^+ source population in the plasma sheet, or equivalently the physics associated with the energization and transport of O^+ to the plasma sheet and ring current. Ebihara et al. [2006] suggest that a significantly larger fraction of escaping ionospheric O^+ reaches the ring current during geomagnetically active times. None of the other existing models explicitly considers activity-dependent O^+ energy and density distributions in the plasma sheet.

Knowledge of the consequences of activity-dependent O^+ transport and energization paths from the ionosphere to the ring current is essential to understanding ring current dynamics. This knowledge cannot be derived directly from observations; rather it has to be obtained by careful use of the data presented here to provide inputs and/or boundary conditions on large-scale magnetospheric models.

Conclusions

We have reported average fluxes and energies of outflowing energetic H^+, O^+, and He^+ ions observed by the Polar/TIMAS instrument in dynamic boundary-related coordinates. These observations were obtained near Polar perigee during quiet geomagnetic intervals at solar minimum. We also presented estimates of the energy of escaping ions that included both the thermal and energetic components of the distributions. We found that at quiet times near the Polar perigee altitude of ~6,000 km, the characteristic energies of escaping H^+ are between 30 and 300 eV in the cusp region and between 30 eV and 1.2 keV in the midnight sector. For O^+ we conclude that the characteristic energy is ~100 eV in the cusp and between 150 and 600 eV in the midnight sector.

Other conclusions from the data presented here are:

- Only a small fraction (~2-3%) of energetic ions escapes directly into the polar cap.

- Energetic ions observed in the polar cap are not only transported there by prevailing convection electric fields, but are also produced by ion acceleration events occurring in the polar cap.

- Estimates of characteristic energies from ratios of energy flux to number flux are most reliable when restricted to the dynamically determined auroral oval.

- The data in Tables 1 and 4 suggest that the relative energization and acceleration of O^+ in the noon quadrant are significantly different from those in other MLT quadrants and that care must be taken in attempts to parameterize O^+ energization as a function of MLT.

- The data presented in Table 2 show that a larger fraction of O^+ is energized above 15 eV at altitudes near Polar perigee (~6,000 km) compared with H^+. This is consistent with the result reported by Peterson et al. [2006] that auroral and cusp energization processes acting between the ionosphere and Polar perigee at ~6,000 km have significant mass dependencies.

The observations and analysis presented above suggest that O^+ has activity-dependent transport paths from the ionosphere to the plasma sheet and on to the ring current. The determination of the possible existence of activity-dependent O^+ transport paths and their consequences cannot be made using existing data and/or models. Knowledge of the effects of slow moving O^+ ions during geomagnetically dynamic times will have to be obtained through the careful use of the data presented here as inputs and/or boundary conditions to large-scale magnetospheric models.

Acknowledgements

References

Andersson, L., W.K. Peterson, and K.M. McBryde (2004) Dynamic coordinates for auroral ion outflow, *J. Geophys. Res.*, 109, A08201, doi:10.1029/2004JA010424.

Andersson, L., W. K. Peterson, and K. M. McBryde (2005) Estimates of the suprathermal O^+ outflow characteristic energy and relative location in the auroral oval, *Geophys. Res. Lett.,* 32, L09104, doi:10.1029/2004GL021434.

Brandt, P. C:son, S. Ohtani, D. G. Mitchell, M.-C. Fok, E. C. Roelof, and R. Demajistre (2002), Global ENA observations of the storm mainphase ring current: Implications for skewed electric fields in the inner magnetosphere, *Geophys. Res. Lett.,* 29, 1954, doi:10.1029/2002GL015160.

Collin, H. L., R.D. Sharp, E.G. Shelley, and R.G. Johnson (1981), Some general characteristics of upflowing ion beams over the auroral zone and their relationship to auroral electrons, *J. Geophys. Res.*, 86, 6820.

Collin, H.L., W.K. Peterson, J.F. Drake, and A.W. Yau (1988), The Helium Components of Energetic Terrestrial Ion Upflows: Their Occurrence, Morphology, and Intensity, *J. Geophys. Res.* 93, 7558.

Collin, H.L.,W.K. Peterson, O.W. Lennartsson, and J.F. Drake (1998), The Seasonal Variation of Auroral Ion Beams, *Geophys. Res. Lett.*, 25, 4071. 1998.

Cully C. M., E. F. Donovan, A. W. Yau, and G. G. Arkos (2003), Akebono/Suprathermal Mass Spectrometer observations of low-energy ion outflow: Dependence on magnetic activity and solar wind conditions, *J. Geophys. Res.*, 108, 1093, doi:10.1029/2001JA009200.

Delcourt, D.C., (2002), Particle acceleration by inductive electric fields in the inner magnetosphere, *J. Atmos. and Solar-Terr. Phys.* 64, 551.

Ebihara, Y., M. Yamada, S. Watanabe, and M. Ejiri (2006), Fate of outflowing
suprathermal oxygen ions that originate in the polar ionosphere, J. Geophys. Res.,
111, A04219, doi:10.1029/2005JA011403.

Feldstein, Y. I., (1963), On Morphology and Auroral and Magnetic Disturbances at High
Latitudes, *Geomagn. Aeron*. 3, 138.

Fok, M.-C., R. A. Wolf, R. W. Spiro, and T. E. Moore (2001), Comprehensive
computational model of Earth's ring current, *J. Geophys. Res.,* 106, 8417.

Hesse, M and J. Birn (2004), On the cessation of magnetic reconnection, *Ann. Geophys.,*
22, 603-612, www.ann-geophys.net/22/603/2004/.

Holzworth, R. H., and C.-I. Meng (1975), Mathematical Representation of the Auroral
Oval, *Geophys. Res. Lett.* 2, 377.

Huddleston, M. M., C. R. Chappell, D. C. Delcourt, T. E. Moore, B. L. Giles, and M. O.
Chandler (2005), An examination of the process and magnitude of ionospheric
plasma supply to the magnetosphere, J. Geophys. Res., 110, A12202,
doi:10.1029/2004JA010401.

Hultqvist, B., M. Øieroset, G. Passman and R. Treuman, Editors, (1999) *Magnetospheric
Plasma Sources and Losses,* Kluwer Academic Publishers, Dordrecht, Boston,
London.

Khazanov, G. V., K. V. Gamayunov, D. L. Gallagher, J. U. Kozyra, and M. W. Liemohn
(2007), Self-consistent model of magnetospheric ring current and propagating
electromagnetic ion cyclotron waves: 2. Wave-induced ring current precipitation and
thermal electron heating, *J. Geophys. Res. 112,* A04209, doi:10.1029/2006JA012033.

Lennartsson, O.W., and E.G. Shelley (1986), Survey of 0.1- to 16-keV/e plasma sheet ion
composition, J. Geophys. Res. 91, 3061.

Lennartsson, O.W., W.K. Peterson, and H.L. Collin (2004), Solar wind control of Earth's
H+ and O^+ outflow rates in the 15-eV to 33-keV energy range, *J. Geophys. Res.,* 109,
A12212 10.1029/2004JA010690.

Lotko, W. (2007), The magnetosphere–ionosphere system from the perspective of plasma
circulation: A tutorial, J. Atmos. and Solar-Terr. Phys., 69, 191.

Mitchell, D.G, P C:Son Brandt, E. C. Roelof, D.C.Hamilton, K C. Retterer, and S. Mende
(2003), Global imaging of O^+ from IMAGE/HENA*, Space Sci. Rev.,*109**, 63.

Miyake, W., T. Mukai and N. Kaya (1993), On the evolution of Ion Conics Along the
Field Line From EXOS D, *J. Geophys. Res*., 98, 11127.

Nilsson, H. et al. (2006), Characteristics of high altitude oxygen ion energization and
outflow as observed by Cluster: A statistical study, *Ann. Geophys*., 24, 1099,
doi:www.ann-geophys.net/24/1099/2006/.

Peterson, W.K., H.L. Collin, M.F. Doherty, and C.M. Bjorklund (1992), O^+ and He^+
restricted and extended (bi-modal) ion conic distributions, *Geophys. Res. Lett.,* 19,
1439.

Peterson, W.K., H.L. Collin, A.W. Yau, and O.W. Lennartsson (2001), Polar/TIMAS
Observations of Suprathermal Ion Outflow During Solar Minimum Conditions, *J.
Geophys. Res.,* 106, 6059.

Peterson, W.K., H.L. Collin, O.W. Lennartsson and A.W. Yau (2006), Quiet time solar
illumination effects on the fluxes and characteristic energies of ionospheric outflow, *J.
Geophys. Res.,* 111, A11S05, doi:10.1029/2005JA011596.

Perez, J. D., X.-X. Zhang, P. C:son Brandt, D. G. Mitchell, J.-M. Jahn, and C. J. Pollock (2004), Dynamics of ring current ions as obtained from IMAGE HENA and MENA ENA images, *J. Geophys. Res.*, 109, A05208, doi:10.1029/2003JA010164.

Roeder, J. L.,M.W. Chen, J. F. Fennell, and R. Friedel (2005), Empirical models of the low-energy plasma in the inner magnetosphere, *Space Weather,* 3, S12B06, doi:10.1029/2005SW000161.

Scudder, J.D., et al. (1995), Hydra – A 3-dimensional electron and ion hot plasma instrument for the Polar Spacecraft of the GGS Mission, *Space Sci. Rev.*, 71, 459.

Shay, M.A., and M. Swisdak (2004), Three-species collisionless reconnection: Effect of O^+ on magnetotail reconnection, *Phys. Rev.Lett*, 93, 175001, doi:10.1103/PhysRevLett.93.175001.

Shelley, E.G., W.K. Peterson, A.G. Ghielmetti, and J. Geiss, (1982), The Polar Ionosphere as a Source of Energetic Magnetospheric Plasma,*Geophys. Res. Let*t. 9, 941.

Shelley, E.G., et al., (1995), The Toroidal Imaging Mass-Angle Spectrograph (TIMAS) for the Polar Mission, *Space Science Reviews,* 71, 497.

Sotirelis, T., and P. T. Newell, Boundary-oriented electron precipitation model, *J. Geophys. Res.,* 105, 18,655, 2000.

Strangeway, R. J., R. E. Ergun, Y.-J. Su, C. W. Carlson, and R. C. Elphic (2005), Factors controlling ionospheric outflows as observed at intermediate altitudes, *J. Geophys. Res.*, 110, A03221, doi:10.1029/2004JA010829.

Su, Y.-J., J.L. Horwitz, T.E. Moore, B.L. Giles, M.O. Chandler, P.D. Craven, M. Hirahara, and C.J. Pollock, (2001), Polar wind survey with the Thermal Ion Dynamics Experiment/Plasma Source Instrument suite aboard POLAR, *J. Geophys. Res.*, 103, 29305.

Tung, Y.-K., C.W. Carlson, J.P. McFadden, D.M. Klumpar, G.K. Parks, W.J. Peria, and K. Liou (2001), Auroral polar cap boundary ion conic outflow observed on FAST, *J. Geophys. Res.,* 106, 3603.

Whalen, B.A., et al. (1990) The Suprathermal Ion Mass Spectrometer (SMS) for the Akebono (EXOS-D) spacecraft, *J. Geomag. Geoelectr.*, 42, 511.

Yau, A.W., W.K. Peterson, and E.G. Shelley (1988), Quantitative Parameterization of Energetic Ionospheric Ion Outflow, in Modeling Magnetospheric Plasma, Geophysical Monograph 44, American Geophysical Union, Washington, DC. 211.

Yau, A.W., T. Abe, and W.K. Peterson (2007), The polar wind: Recent observations, *J. Atmos. and Solar-Terr. Phys*. 69, 1936.

Zheng, Y., T. E. Moore, F. S. Mozer, C. T. Russell, and R. J. Strangeway (2005), Polar study of ionospheric ion outflow versus energy input, *J. Geophys. Res.*, 110, A07210, doi:10.1029/2004JA010995.

Table 1. Net upflowing hemispheric fluxes (in 10^{24} ions s^{-1}), flux ratios, and UFI percentage for different MLT and latitude regions*

			Flux or Ratio - All ions					Flux or Ratio - UFI					UFI %				
			All MLT	Noon	Dusk	Midnight	Dawn	All MLT	Noon	Dusk	Midnight	Dawn	All MLT	Noon	Dusk	Midnight	Dawn
H+	I	All Latitudes	1.54	0.44	0.09	0.59	0.42	1.21	0.22	0.2	0.49	0.31	79%	50%	222%	83%	74%
	D	All Latitudes	1.34	0.42	0.16	0.53	0.23	0.93	0.18	0.15	0.45	0.16	69%	43%	94%	85%	70%
		Polar Cap	0.03	0.005	0.004	0.01	0.01	0.02	0.002	0.003	0.006	0.006	67%	40%	75%	60%	60%
		Auroral Zone	1.31	0.41	0.15	0.52	0.22	0.91	0.18	0.14	0.44	0.15	69%	44%	93%	85%	68%
		Polar Cap/All Lat	*2.2%*	*1.2%*	*2.5%*	*1.9%*	*4.3%*	*2.2%*	*1.1%*	*2.0%*	*1.3%*	*3.8%*					
O+	I	All Latitudes	2.41	0.86	0.17	0.84	0.53	2.01	0.64	0.22	0.66	0.5	83%	74%	129%	79%	94%
	D	All Latitudes	1.71	0.67	0.18	0.46	0.4	1.38	0.51	0.17	0.38	0.33	81%	76%	94%	83%	83%
		Polar Cap	0.05	0.01	0.003	0.006	0.03	0.04	0.009	0.002	0.004	0.02	80%	90%	67%	67%	67%
		Auroral Zone	1.66	0.66	0.18	0.46	0.36	1.34	0.5	0.16	0.38	0.3	81%	76%	89%	83%	83%
		Polar Cap/All Lat	*2.9%*	*1.5%*	*1.7%*	*1.3%*	*7.5%*	*2.9%*	*1.8%*	*1.2%*	*1.1%*	*6.1%*					
He+	I	All Latitudes	0.17	0.02	0.03	0.07	0.05	0.11	0.02	0.02	0.04	0.03	65%	100%	67%	57%	60%
	D	All Latitudes	0.13	0.03	0.01	0.07	0.03	0.08	0.01	0.008	0.04	0.02	62%	33%	80%	57%	67%
		Polar Cap	0.004	0.0003	0.001	0.002	0.0006	0.002	0.0001	0.0006	0.001	0.0002	50%	33%	60%	50%	33%
		Auroral Zone	0.13	0.03	0.009	0.07	0.02	0.07	0.01	0.007	0.04	0.02	54%	33%	78%	57%	100%
		Polar Cap/All Lat	*3.1%*	*1.0%*	*10.0%*	*2.9%*	*2.0%*	*2.5%*	*1.0%*	*7.5%*	*2.5%*	*1.0%*					

* I = static (invariant) coordinates; D = dynamic (boundary-related) coordinates; columns 4-8: all ions; columns 9-13: UFI only; columns 14-18: UFI percentage

Table 2 Total upward hemispherical fluxes from various platforms at various altitudes obtained over various energy ranges from the indicated sources, in units of 10^{24} s^{-1}, and estimates of fraction of thermal flux below the low energy threshold at two altitudes. The thermal flux values shown are upper limits as described in the text.

Source	Altitude (km)	Energy (keV)	H+			O+			He+	
			Measured Flux	<15 eV at 5,000 km	<15 eV at 50,000 km	Measured Flux	<15 eV at 5,000 km	<15 eV at 50,000 km	Measured Flux	<15 eV at 50,000 km
FAST[1]	3000	0.003- 12	-	-	-	2	41%	82%	-	-
This Report	6000	0.015- 33	1.34	93%	99%	1.71	45%	84%	0.13	95%
Polar/TIMAS[2]	6000	0.015- 33	3	85%	98%	3	31%	75%	0.2	93%
Akebono[3]	9000	0.000-0.07	2	n/a	n/a	2	n/a	n/a	-	-
DE[4,5]	20000	0.010-17	10	64%	93%	7	16%	56%	0.8	77%
Polar/TIMAS[6]	50000	0.015- 33	10	64%	93%	15	8%	38%	-	-
Polar/TIDE[7]	5000	thermal	17	-	-	1.4	-	-	-	-
Polar/TIDE[8]	5000	thermal	87	-	-	-	-	-	-	-
Polar/TIDE[7]	50000	thermal	131	-	-	9	-	-	2.7	-

[1]Andersson et al. [2005], [2]Peterson et al. [2006], [3]Cully et al. [2003], [4]Yau et al., [1988], [5]Collin et al. [1988], [6]Lennartsson et al. [2004], [7]Su et al. [1998], and [8]Huddleston et al. [2005]

Table 3 Estimates of characteristic energy of ions from the auroral zone (AZ) and polar cap (PC), in units of keV.

		Energy 0.015-33 keV	Energy (UFI) 0.015-33 keV	Number Flux Below 15 eV (50,000)	Estimated Energy 0-33 keV
H^+	PC	1.5	0.3	99.97%	0.001
	AZ	0.9	0.56	97.0%	0.03
O^+	PC	0.82	0.19	99.1%	0.008
	AZ	0.28	0.30	63.8%	0.1
He^+	PC	3	0.7	99.8%	0.008
	AZ	0.8	0.6	87.1%	0.11

Table 4 Estimates of characteristic energies of escaping ionospheric ions in the four MLT auroral zone quadrants, in units of keV.

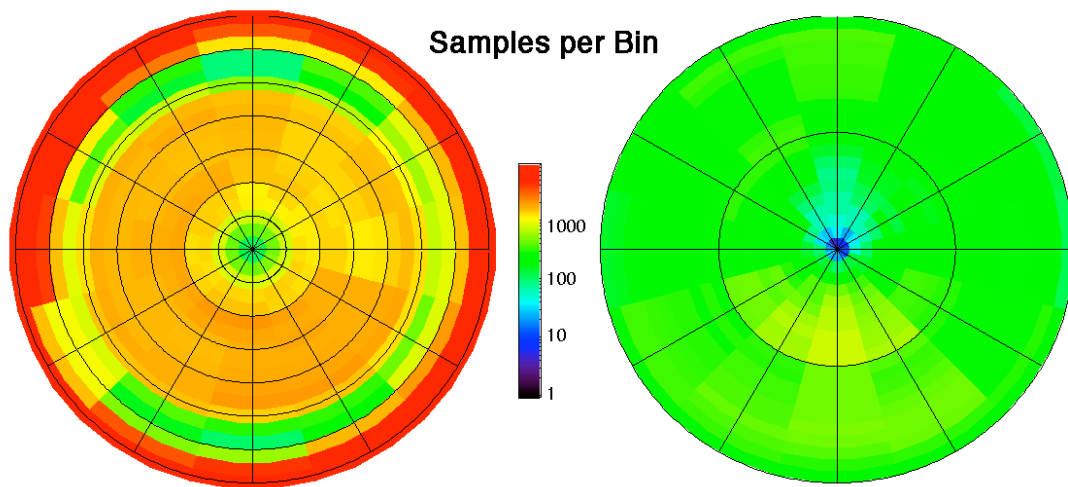|		Noon	Dusk	Midnight	Dawn
H^+	TIMAS Energy	0.27	1.60	1.15	0.94
	UFI Energy	0.20	0.31	0.88	0.30
	Corrected Energy	0.03	0.03	0.03	0.02
O^+	TIMAS Energy	0.12	0.33	0.59	0.17
	UFI Energy	0.12	0.41	0.59	0.18
	Corrected Energy	0.09	0.08	0.15	0.06
He^+	TIMAS Energy	0.19	0.59	1.33	0.27
	UFI Energy	0.24	0.60	0.85	0.36
	Corrected Energy	0.05	0.05	0.05	0.05

Figures and captions:

Figure 1. Number of observation samples in invariant latitude / magnetic local time bins from 54° to 90° INVL (left) and in boundary-related latitude / magnetic local time bins in the auroral zone and polar cap (right). The number of samples in each bin is encoded by the color bar. Magnetic noon is at the top and dusk is at the right in each dial. The boundary-related latitude bins in the auroral zone and polar cap are outside and inside the heavy black circle, respectively, in the right panel. Note that the actual shape of the auroral oval is not circular in contrast to the circular shape depicted on the right panel and in the other figures. The auroral oval is narrowest near noon and widest near midnight and the average width increases with increasing geomagnetic activity.
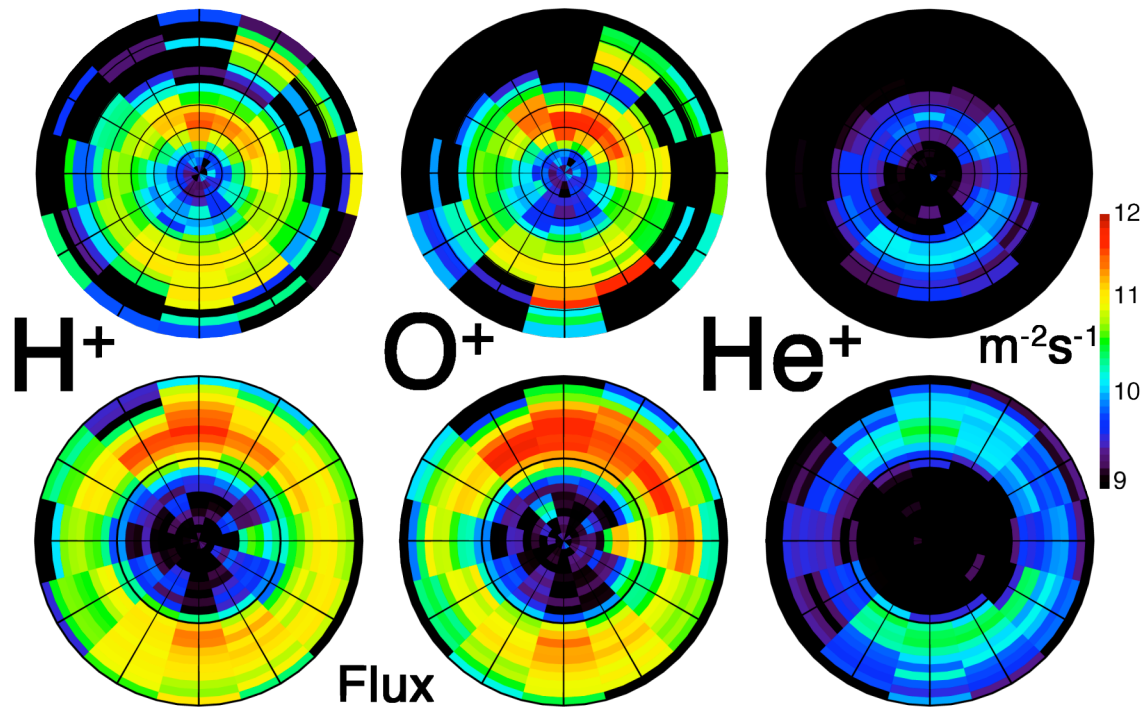
Figure 2. Net hemispheric upflowing flux of H^+ (left), O^+ (middle) and He^+ (right) energetic ions observed during geomagnetically quiet intervals (i.e. Dst > -50) from March 1996 to December 8, 1998, in units of $(m^2s)^{-1}$. Data are displayed in fixed INVL/MLT coordinates on the top row and dynamic boundary related coordinates in the bottom row. Net upflowing number fluxes are encoded using the color bar on the right. The coordinate systems are the same as those displayed in Figure 1. Magnetic noon is at the top of each dial and the invariant latitude runs from 54 to 90 degrees in the top row. Note that the auroral oval is not circular as depicted in the bottom panels and other figures; see text for a discussion of this point.
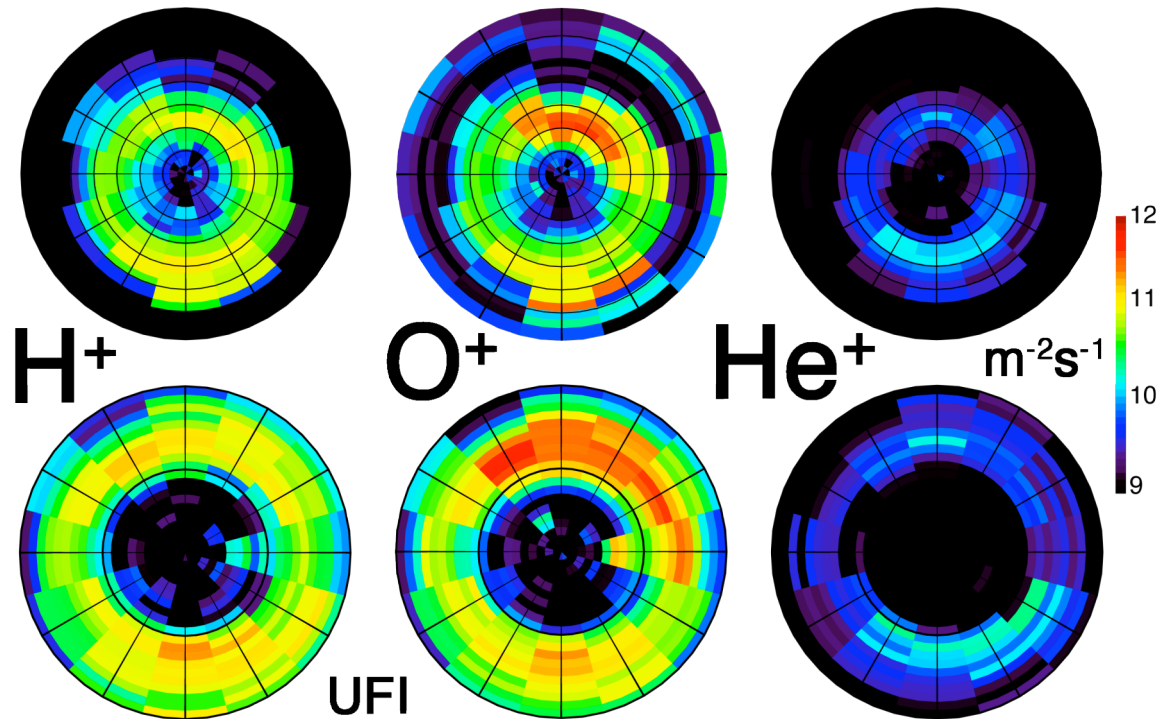
Figure 3. Net hemispheric upflowing flux of H$^+$ (left), O$^+$ (middle) and He$^+$ (right) upflowing ion (UFI) distributions observed during geomagnetically quiet intervals from March 1996 to December 8, 1998, i.e. energetic ions in which the angular distributions have well defined peaks. Same data display format as in Figure 2. Magnetic noon is at the top of each dial and the invariant latitude runs from 54 to 90 degrees in the top row. Note that the auroral oval is not circular as depicted in the bottom panels and other figures; see text for a discussion of this point.
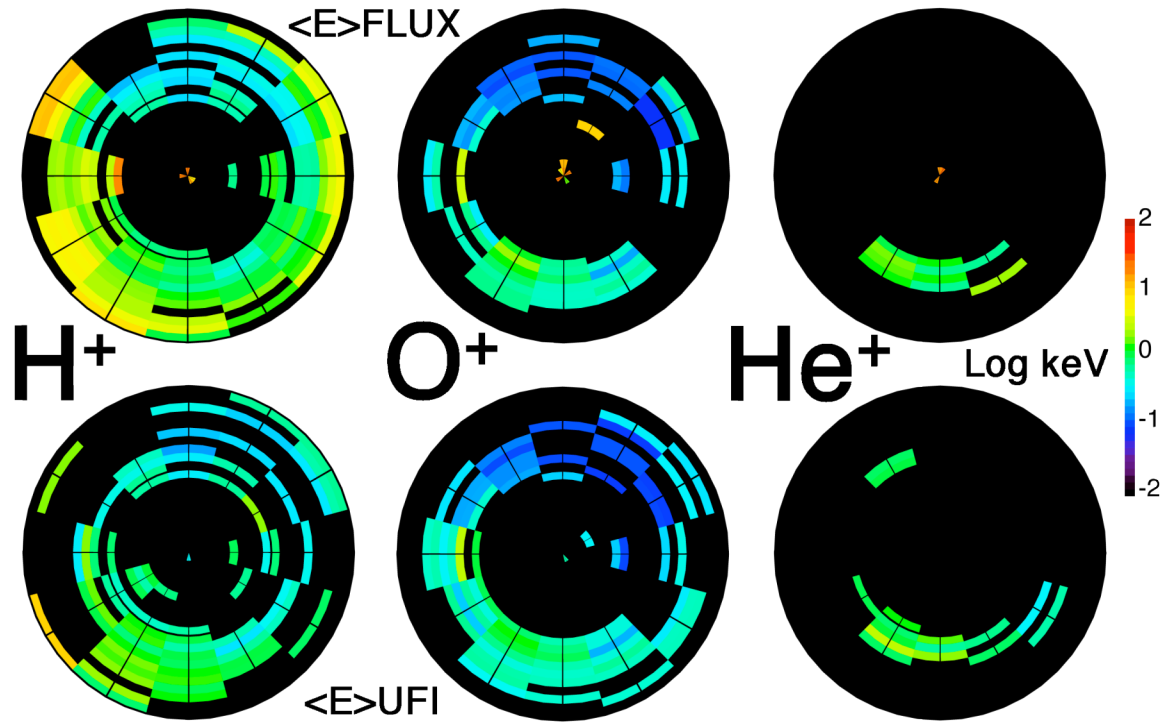
Figure 4. Distribution of characteristic energy derived from the ratio of energy flux to number flux in dynamic boundary-related coordinates for the flux data shown in Figure 2 and the UFI data shown in Figure 3. The characteristic energy is encoded in the color bar on the right. Black pixels indicate latitude/MLT bins where the characteristic energy was less than two standard deviations from the energy determined from instrumental count rates. The coordinate systems are the same as those displayed in Figure 1. Magnetic noon is at the top of each dial and the invariant latitude runs from 54 to 90 degrees in the top row. Note that the auroral oval is not circular as depicted in the bottom panels and other figures; see text for a discussion of this point.